nature energy

SUPPLEMENTARY INFORMATION

ARTICLE NUMBER: 16119 | DOI: 10.1038/NENERGY.2016.119

A high-capacity and long-life aqueous rechargeable zinc battery using a metal oxide intercalation cathode

Dipan Kundu, Brian D. Adams, Victor Duffort, Shahrzad Hosseini Vajargah

*and Linda F. Nazar**

Department of Chemistry and the Waterloo Institute for Nanotechnology, University of Waterloo,

Waterloo Ontario Canada N2L 3G1

Corresponding Author: lfnazar@uwaterloo.ca

DOI: 10.1038/NENERGY.2016.119

Supplementary Figures

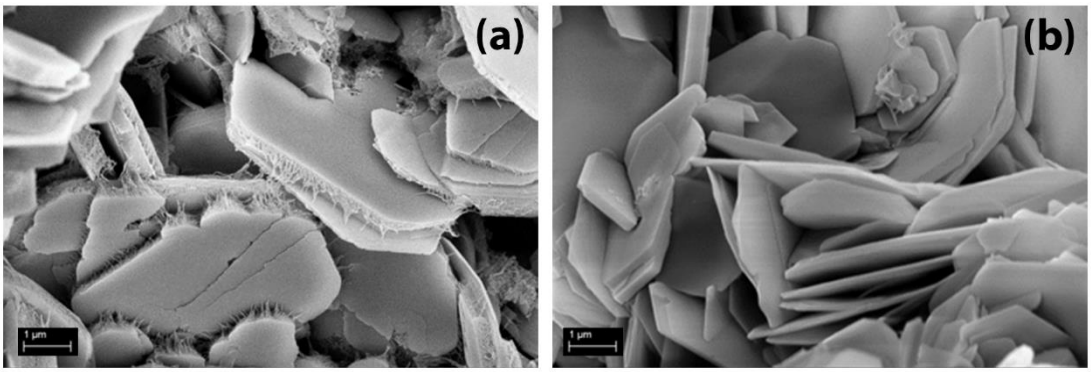

Supplementary Figure 1 | Scanning electron microscope (SEM) images of the Zn electrode surfaces. SEM images of the Zn electrodes after cycling a zinc//1 M $ZnSO_4$//zinc symmetrical cell at a current density of 10 mA cm^{-2} with a deposition and stripping cut-off capacity limitation of 1 mAh cm^{-2} for 25 cycles. (a) shows the surface of the zinc-deposited electrode and (b) shows the surface of the stripped electrode.

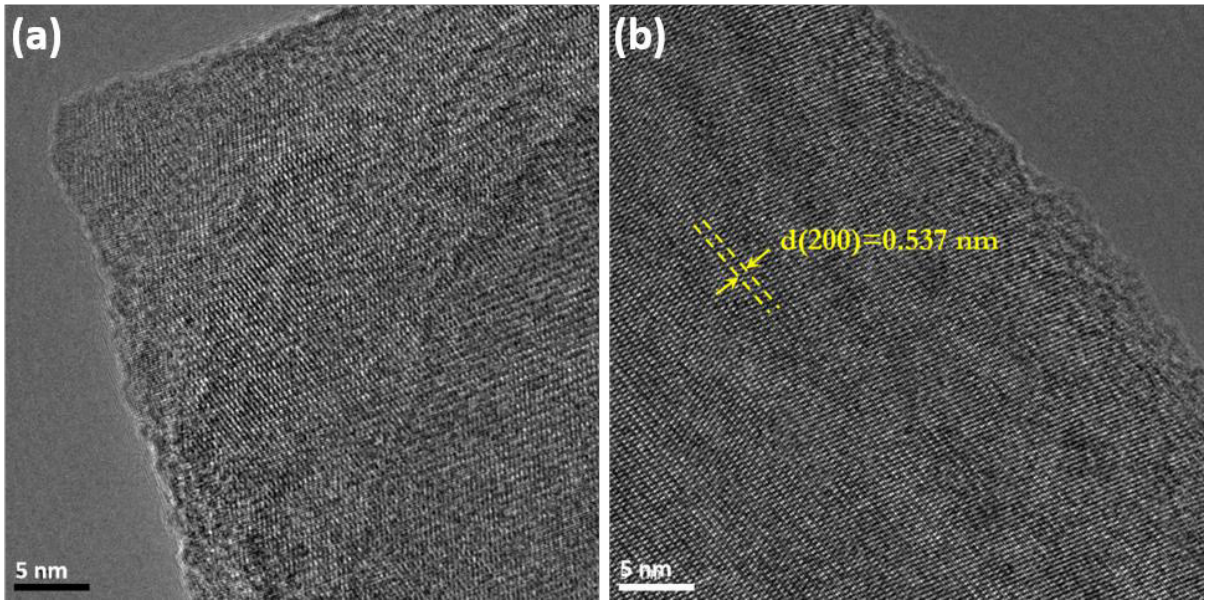

Supplementary Figure 2 | High resolution transmission electron microscopy imaging of the $Zn_{0.25}V_2O_5.nH_2O$ nanobelts. (a) A representative TEM image of a section of a nanobelt with a flat ribbon-like morphology. (b) HRTEM image of the (200) lattice fringes running parallel to the growth direction (long axis) of the nanobelts.

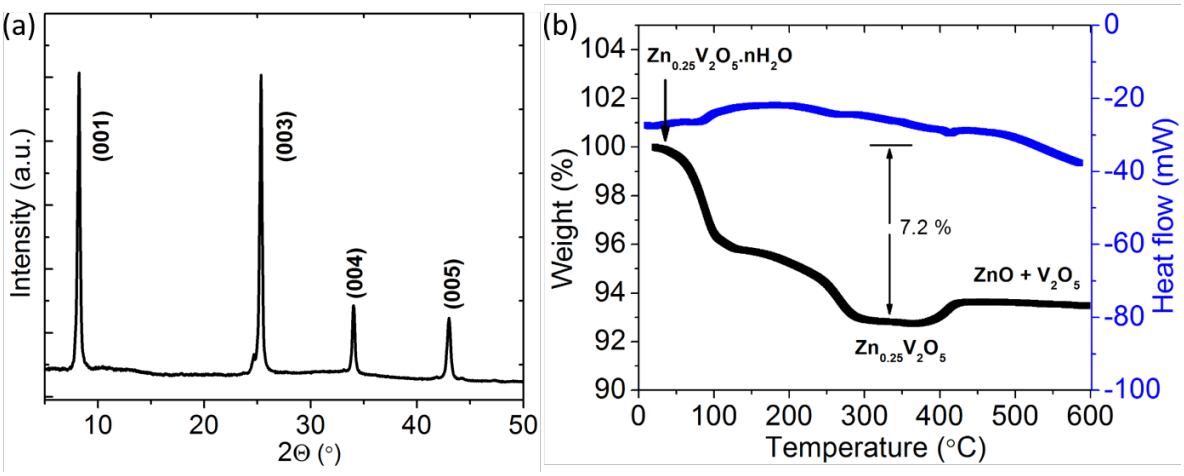

Supplementary Figure 3 | Characterization of the as-synthesized $Zn_{0.25}V_2O_5.nH_2O$ nanobelts. (a) XRD pattern showing the (*00l*) set of peaks due to the high degree of preferred orientation of the nano-ribbon morphology with the ***c*** axis perpendicular to the sample surface. (b) TGA-DTA analysis of the pristine nanobelts showing stepwise loss of lattice water corresponding to an overall 7.2 % weight loss, equivalent to 0.85 molecule of water per formula unit.

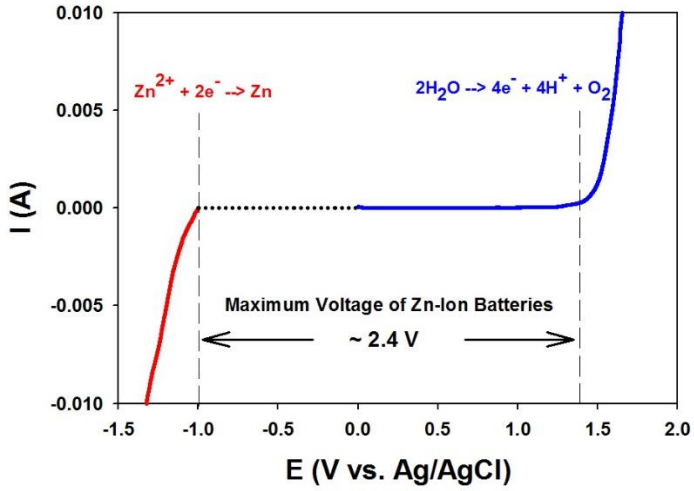

Supplementary Figure 4 | Working potential window of an aqueous zinc ion battery using 1M $ZnSO_4$ in water as the electrolyte. Data was obtained from linear sweep voltammetry analysis on a Zn disc and a stainless steel (SS) disc electrode, respectively, at a 1 mV/s scan rate against a Ag/AgCl reference electrode. The cathodic sweep shows the Zn deposition on Zn and the anodic sweep shows water oxidation (O_2 evolution) on the SS electrode.

DOI: 10.1038/NENERGY.2016.119

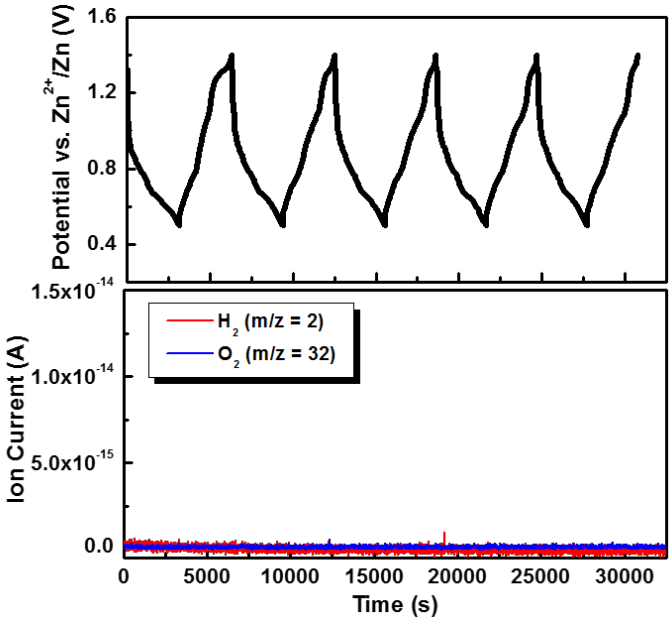

Supplementary Figure 5 | *Operando* H_2 and O_2 evolution analysis of the Zn||$Zn_{0.25}V_2O_5.nH_2O$ cell using *operando* electrochemical mass spectrometry (OEMS). The Swagelok® type cell was galvanostatically cycled in 1M $ZnSO_4$-H_2O as the electrolyte in 0.5 – 1.4 V window and gas evolution was monitored in *operando* by quantitative OEMS. As evident, no ion current corresponding to H_2 and O_2 could be detected during cell operation confirming the stability of the aqueous electrolyte in the voltage window of operation.

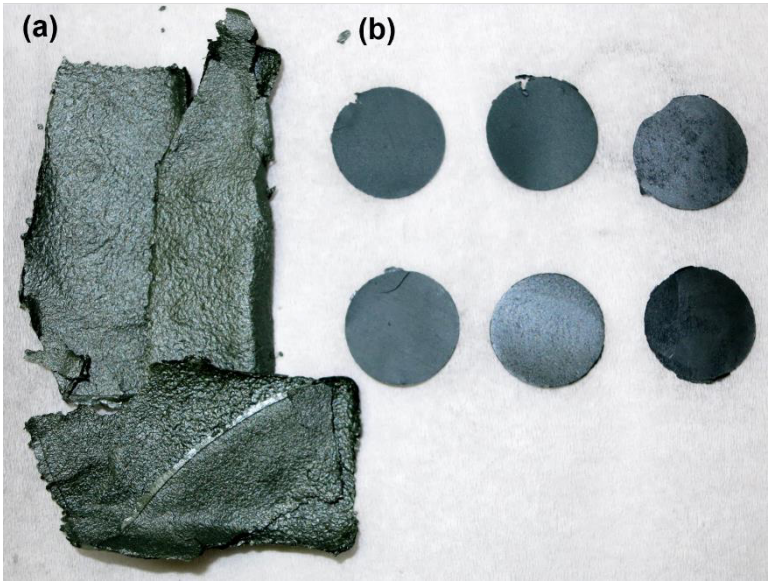

Supplementary Figure 6 | Representative photographs of $Zn_{0.25}V_2O_5.nH_2O$ free standing membranes. (a) as-synthesized material and (b) examples of punched freestanding electrodes.

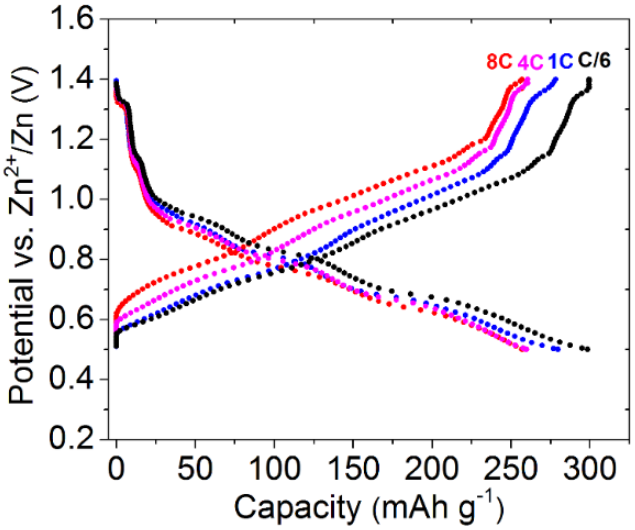

Supplementary Figure 7 | Electrochemistry of the Zn||$Zn_{0.25}V_2O_5.nH_2O$ cell. Galvanostatic discharge-charge polarization curves of the $Zn_{0.25}V_2O_5.nH_2O$ positive electrode at C/6, 1C, 4C and 8C rate (1C = 300 mA g^{-1}). For the 4C and 8C rates, the highest capacity cycle is plotted here for comparison.

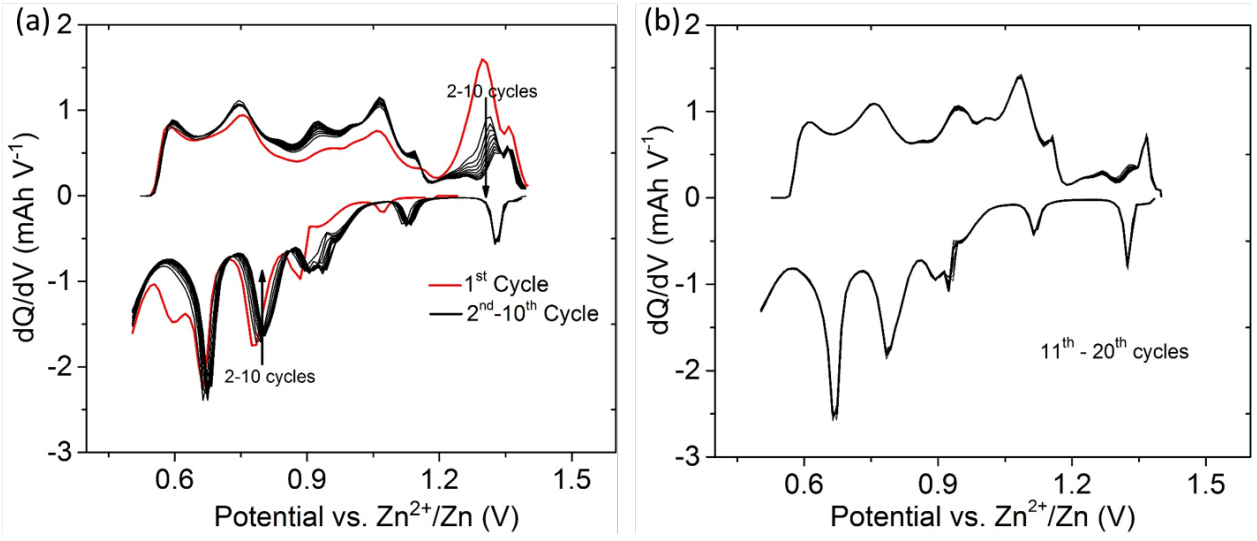

Supplementary Figure 8 | Differential capacity plots of the Zn||$Zn_{0.25}V_2O_5.nH_2O$ cell. The plots are the derivative of the galvanostatic discharge-charge curves obtained at a 1C rate shown in Fig. 4a, and show (a) changes within the first 10 cycles that indicate initial evolution of cathodic and anodic processes, followed by (b) stabilization over subsequent cycling.

DOI: 10.1038/NENERGY.2016.119

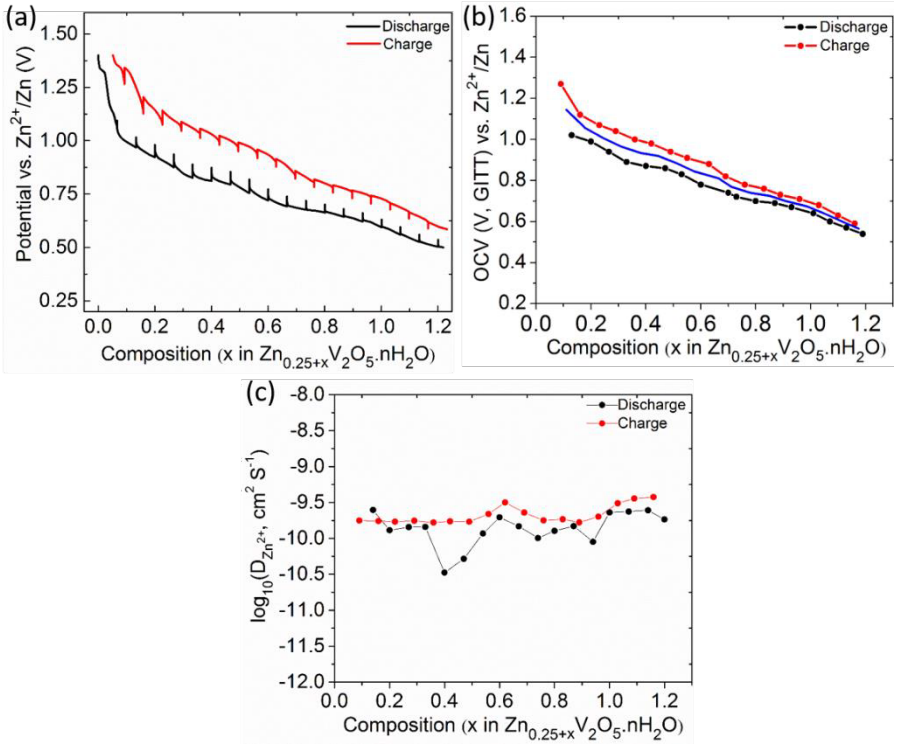

Supplementary Figure 9 | Galvanostatic intermittent titration (GITT) profiles and resulting diffusion coefficient data for $Zn_{0.25}V_2O_5.nH_2O$ in aqueous electrolyte solution. (a) Discharge/charge GITT curves for the $Zn_{0.25}V_2O_5.nH_2O$ electrode; (b) equilibrium potential vs. Zn^{2+} ion composition in the $Zn_{0.25}V_2O_5.nH_2O$ electrode obtained using the GITT technique (see above). The median value for the equilibrium voltage is ~0.8 V; (c) Diffusion coefficients as a function of the Zn^{2+} composition during discharge/charge of the $Zn_{0.25}V_2O_5.nH_2O$ electrode obtained by applying the GITT technique (for details see discussion below).

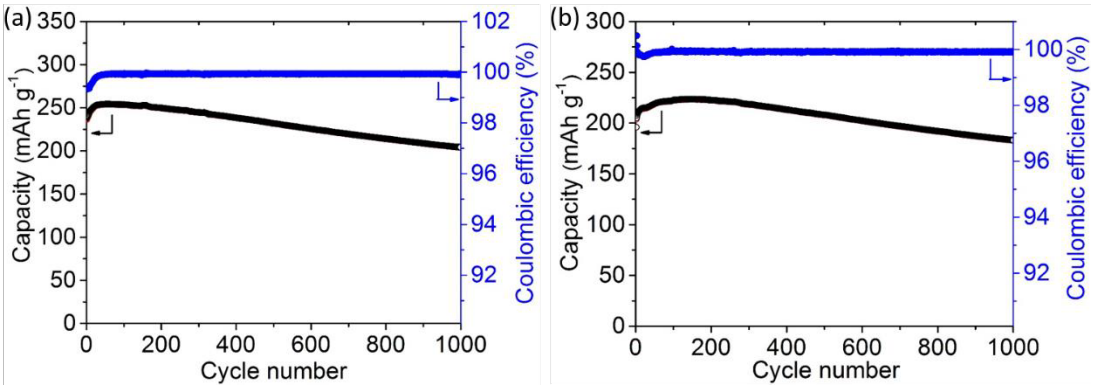

Supplementary Figure 10 | High rate, long term cycling for $Zn_{0.25}V_2O_5.nH_2O$. Capacity as a function of cycle number and the corresponding coulombic efficiency at (a) 10 C and (b) 15 C rates.

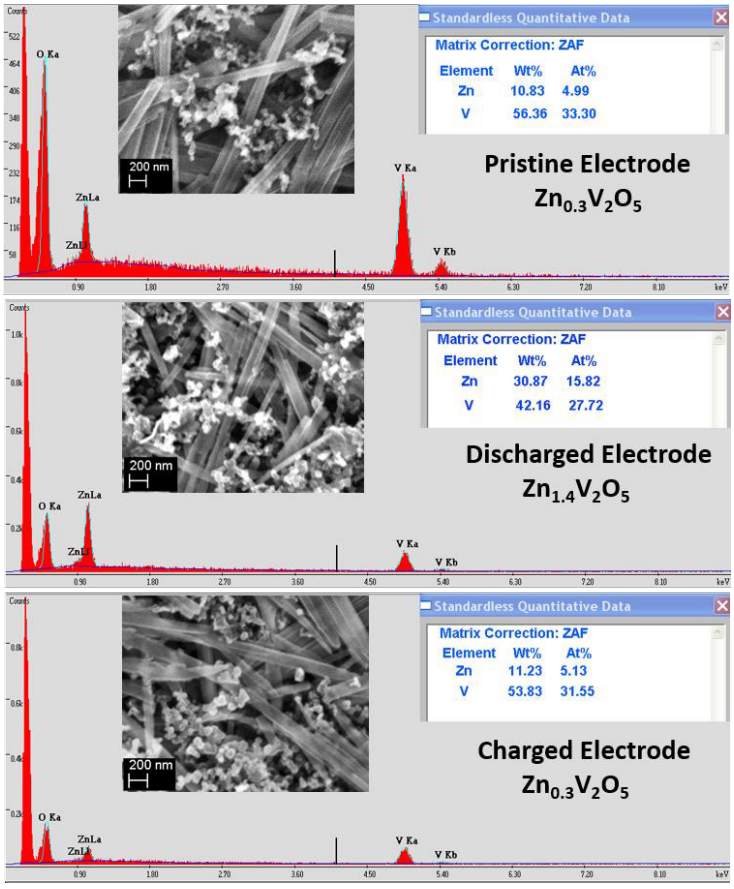

Supplementary Figure 11 | Energy dispersive X-ray spectroscopy and SEM analysis of the pristine, discharged and charged positive electrode and quantification of the Zn to V ratio. The Zn content increases by 1.1 per formula unit from the pristine to the discharged electrode before decreasing by same after charge. EDX analysis showed slightly higher (0.05) Zn content in the electrodes compared to that obtained by ICP analysis. Electrodes were discharged/charged at 1C (300 mA g^{-1}) rate.

DOI: 10.1038/NENERGY.2016.119

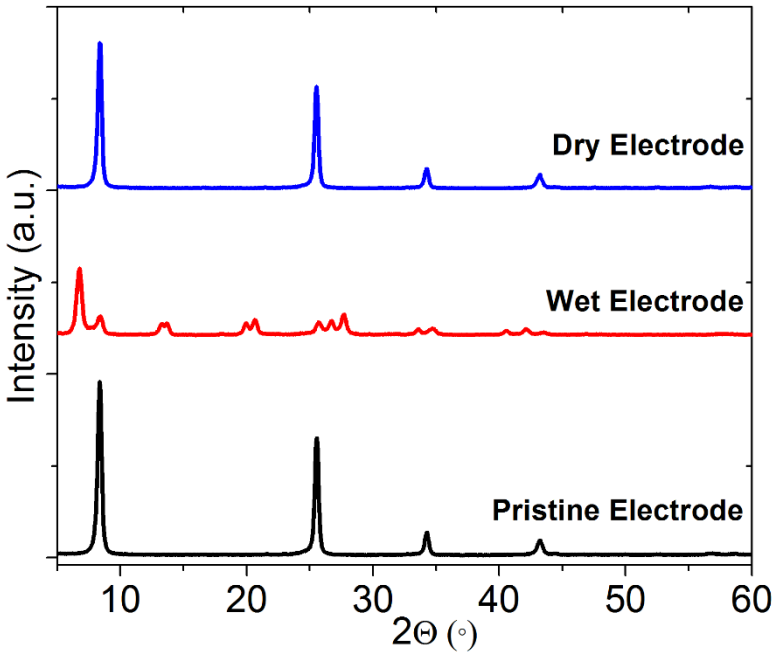

Supplementary Figure 12 | XRD patterns of the wet and dried positive $Zn_{0.25}V_2O_5.nH_2O$ electrode.

Supplementary Figure 13 | Pouch cell used for the ICP-OES analysis of the cycled electrolyte.

Supplementary Tables

Supplementary Table 1. Inductively Coupled Plasma Optical Emission Spectroscopy (ICP-OES) analysis: Zn/V compositions obtained for the pristine $Zn_{0.25}V_2O_5.nH_2O$, and discharged/charged electrodes in the second cycle. Electrodes were discharged/charged at 1C (300 mA g^{-1}) rate. At this rate a discharge/charge capacity of 275 mAh g^{-1} was obtained in the second cycle.

Sample	Zinc (mmol/L) x 10^2	Vanadium (mmol/L) x 10^2	Zn/V
Pristine sample	9.93	81.13	0.25/2
Discharged electrode	19.78	28.53	1.39/2
Charged electrode	4.69	30.45	0.3/2

Supplementary Notes

1. Investigation of the cycled Zn electrode

Supplementary Fig. 1 clearly shows that the typical dendritic formations, which are classic to zinc deposition in alkaline electrolytes, do not occur with the near-neutral 1 M $ZnSO_4/H_2O$ electrolyte, even at high current density (10 mA/cm^2). The morphology of electrodeposited zinc is dependent on the zincate ($Zn(OH)_4^{2-}$) intermediate in alkaline media.[1] Precipitation of zincate at the surface of the zinc electrode generally initiates dendritic morphologies due to non-uniform concentration gradients.[2] At neutral pH (or slightly acidic: pH of 1 M ZnSO4/H2O ~ 4-5), where no zincate ions are present, the deposition process is much simpler ($Zn^{2+} + 2e^- \rightarrow Zn$) and no dendritic deposits are observed. As can be seen in Supplementary Fig. 1a and 1b, after 25 cycles, both electrode surfaces look quite similar. Massive hexagonal plates are formed after cycling which are stacked randomly. Deposition occurs preferentially at the plate edges as can be seen by the roughened edges in (a) relative to the smooth surfaces in (b). This symmetrical cell was operated with no pressure or separator, so it can be expected that the growth of the plates will be influenced by those factors. In our work, using glass fiber separators, we did not observed any short-circuits by dendrite formation, even at very high rates. We note that ceramic separators have the mechanical stability to resist puncture by these zinc plates and it is expected that typical microporous membranes used in commercial Li-ion battery technologies will also function similarly.

DOI: 10.1038/NENERGY.2016.119

2. Powder XRD refinement for $Zn_{0.25}V_2O_5.nH_2O$ nanobelts (well-ground)

Diffractometer:	Bruker D8 advance
Radiation	Cu Kα
2θ range (°)	5-80
Step size (°)	0.025
Sec/step	4
Background	Chebyshev Polynomial
Chemical formula	$Zn_{0.25}V_2O_5.nH_2O$ (n = 1.0)
Space group	$P\bar{1}$
a (Å)	10.75(2)
b (Å)	7.77(1)
c (Å)	10.42(4)
α (°)	91.26(2)
β (°)	90.31(5)
γ (°)	88.66(1)
Cell Volume ($Å^3$)	870.98(2)
Crystallite Size (nm)	236(3)
R_{wp} [%]	2.799
χ^2 (gof)	3.769

Atomic positions and occupancies were not refined due to the high degree of preferred orientation present in the diffraction data.

3. ICP-OES analysis of cycled electrolyte

Quantification of oxide dissolution over long term electrochemical cycling was investigated by Inductively Coupled Plasma – Optical Emission Spectroscopy (ICP-OES) analysis. For this study, a pouch cell was fabricated (Supplementary Fig. 13) and electrochemically cycled at a 1C rate for over 100 cycles. The electrolyte was extracted by washing the electrodes and separator with water to result in a 25 ml solution, which was subjected to ICP-OES analysis. A vanadium concentration of 0.577 mg/L was detected, which is equivalent to 0.01 (4) mg of vanadium in the 25 ml of the pouch cell extract. This only represents 0.01% of the positive electrode material, and therefore active material dissolution does not significantly contribute to capacity fade.

4. Calculations to estimate metrics of the $Zn \| Zn_{0.25}V_2O_5.nH_2O$ cell

Specific Energy of the $Zn \| Zn_{0.25}V_2O_5.nH_2O$ cell: Based on the reversible reaction at a 1C rate: $Zn_{0.25}V_2O_5.nH_2O + 1.1Zn^{2+} + 2.2e^- \leftrightarrow Zn_{1.35}V_2O_5.nH_2O$ and an average voltage of 0.8 V for the rechargeable zinc-ion battery, a specific energy of 175 Wh/kg is calculated for the total active mass, including both positive and negative electrodes.

Volumetric energy density of the Zn‖$Zn_{0.25}V_2O_5.nH_2O$ cell: The $Zn_{0.25}V_2O_5.nH_2O$ positive electrode has a specific capacity of 300 mAh/g and a density of 3.13 g/cm^3. The zinc metal has a specific capacity of 820 mAh/g and its density is 7.14 g/cm^3. A positive electrode thickness of 200 µm which contains 80% active material (i.e. a porosity of 20%) provides 15.49 mAh/cm^2. To match this capacity, the required negative electrode thickness is 26.4 µm. Assuming a combined thickness for current collectors, excess zinc, and separators of 50 µm, the cell level volumetric energy density is estimated to be 450 Wh/L.

Estimation of cost for negative and positive electrode materials: Considering only the mean price of the raw materials, for zinc (USD \$2 /kg)[2] and vanadium pentoxide (USD \$15/kg),[3] the estimated combined cost for the negative and positive can be calculated from the positive in its discharged state ($Zn_{1.35}V_2O_5$). The product would cost approximately USD \$10.75/kg. With a specific energy of 175 Wh/kg, the total bulk material cost for the negative and positive would be as low as \$60/kWh. While historically the V_2O_5 market price has been quite volatile, it somewhat stabilized in 2004, and the estimates above reflect the median prices over the past decade. At today's current price of V_2O_5 (USD \$5.5/kg),[3] the total bulk material cost drops to \$25/kWh. The cost of the 1 M $ZnSO_4/H_2O$ electrolyte is negligible when comparing this technology to batteries operating with a non-aqueous electrolyte. Additional costs would clearly arise from cell components and housing, along with manufacturing cost for the positive electrode which is anticipated to be low owing to the aqueous processing method (see main text).

5. Galvanostatic Intermittent Titration Study

The Galvanostatic Intermittent Titration Technique (GITT) was applied to determine the thermodynamic voltage-composition relationship, which corresponds to the equilibrium phase diagram of the system. The Zn^{2+} ion diffusion coefficients (D_{Zn}^{2+}) in $Zn_{0.25}V_2O_5.nH_2O$ were calculated from the GITT data. In the GITT method the transient voltage generated due to the application of a current pulse is monitored as a function of time. In our study, a galvanostatic pulse (charge or discharge) of 20 min at a 50 mA g^{-1} rate - followed by a 3 h open circuit step to allow relaxation back to equilibrium (defined as < 2 mV/h) - was repeatedly applied until the discharge (charge) voltage reached 0.5 V (1.4 V) vs. Zn. Supplementary Fig. 9a shows the potential vs. composition profile obtained from the GITT experiment. About 1.2 Zn^{2+} ions were (de)intercalated during the complete discharge-charge segment of the GITT process. Supplementary Fig. 9b depicts the variation of equilibrium potential (OCV) with composition (x in $Zn_{0.25+x}V_2O_5$), obtained by

DOI: 10.1038/NENERGY.2016.119

plotting the steady state voltage at the end of each open circuit step. The blue line depicts the average equilibrium potential, and its difference from the discharge/charge OCV profile represents the equilibrium voltage polarization which decreases with increase in Zn^{2+} composition. The sloping nature of the OCV profile indicates that the Zn^{2+} extraction/insertion proceeds predominantly as a single phase reaction. This also allows the application of GITT for the determination of Zn^{2+} diffusion coefficients, which were calculated by the following formula first outlined by Weppner and Huggins:[4]

$$D_{Zn2+}{}^{GITT} = (4/\pi\tau) * [n_M V_M/S]^2 [\Delta E_S/\Delta E_t]^2 \quad (1)$$

Here, τ is the constant current pulse duration (20 min); n_M and V_M are the moles of $Zn_{0.25}V_2O_5.nH_2O$ and molar volume (69 cm^3 mol^{-1}), respectively; S is the electrode-electrolyte interface area (taken as the geometric area of the electrode); ΔE_S, and ΔE_t are the change in the steady state voltage and overall cell voltage after the application of a current pulse in a single step GITT experiment, respectively. We assume the true surface area is higher than the geometric electrode area owing to the material's morphology (which would lower the "true" diffusion coefficient by an order of magnitude), but the geometric electrode area is typically used in such reported calculations and thus favours comparison with other materials. The BET surface area could not accurately assessed owing to the crystalline water in $Zn_{0.25}V_2O_5.nH_2O$ that renders outgassing impossible.

6. X-ray photoelectron spectroscopy (XPS) analysis

XPS analysis was performed on a Thermo ESCALAB 250 instrument configured with a monochromatic Al Kα (1486.6 eV). Spectra were analyzed using CasaXPS software. For the background, a Shirley (vanadium and oxygen) or a Tougaard type function was used. A combination of Gaussian (Y%)-Lorentzian (X%) peak shape functions, defined as GL(X) in CasaXPS was used to fit each component. The suitable mixture of Gaussian-Lorentzian components depends on the natural line-width of the specific core hole and also on the instrument and resolution settings used. In our analysis, for Zn 2p and O 1s spectra, GL(30) was used, whereas for the V 2p region, the best fit was obtained with GL(90), in accordance with the literature.[5] The binding energy values were all calibrated using the adventitious C 1s peak at 284.8 eV. For the fitting of the 2p (V and Zn) component pairs, a peak area ratio of 2:1 for $2p_{3/2}$: $2p_{1/2}$ was used with $2p_{1/2}$ having the higher value of FWHM (full width at half maximum).

For the pristine and the charged positive electrode the V 2p signal was deconvoluted into the V^{4+} ($2p_{3/2}$: 515.8 eV) and V^{5+} ($2p_{3/2}$: 517.3 eV) contributions, which confirms partial reduction

of the V_2O_5 framework due to the presence of indigenous Zn^{2+}. Analysis of the discharged positive electrode revealed a third contribution at 515.3 eV corresponding to V^{3+}, with an increase in intensity of the V^{4+} component as a result of Zn^{2+} intercalation and consequent reduction of V_2O_5 framework. The V^{4+} and V^{5+} components of the discharged electrode shift slightly to higher binding energies of 516.8 eV and 519 eV (V $2p_{3/2}$), respectively. The reason for such a blue shift may be linked to the intercalation of the Zn^{2+} ions and the concomitant bonding rearrangements at the V^{4+}/V^{5+} sites, the exact nature of which still remains unclear. The relative shift of the $V^{4+}$and V^{5+} components also results in two distinct oxide O 1s components (529.26 and 530.12 eV) for the discharged electrode, in contrast to the single broad O 1s peak observed for the pristine and the charged electrode. The high energy O 1s region between 531-534 eV corresponds to the signal from intercalated water, whose presence is evident in the *operando x-ray* diffraction study (refer to the main text).

Supplementary Methods

1. *Operando* mass spectrometry analysis

Operando H_2 and O_2 evolution analysis was performed with a modified design based on an online electrochemical mass spectrometry apparatus reported by Tsiouvaras et. al (*J. Electrochem. Soc.* **160**, A471-A477 (2013)**)**. A Swagelok® type electrochemical flow cell (EL-Cell, ECC-DEMS) is attached in-line with a gas flow controller (Bronkhurst, F-200CV) and a quadrupole mass spectrometer (Standford Research Systems, RGA 200). During cell operation a controlled flow of Ar (5.0 Grade) sweeps the evolved gases from the cell to the MS entrance chamber where the gas enters the quadrupole through a fused silica capillary (50 um ID). The pressure inside the MS chamber is 2×10^{-6} torr during operation. Prior to measurement, the mass spectrometer is calibrated to establish a relationship between the measured ion current (A) and target gas concentration (ppm). With the use of known gas concentrations (from 2000 ppm O_2/Ar balance and 2000 ppm CO_2/Ar balance mixtures) mixed with different amounts of Ar, a linear relationship between the gas concentration and ion current is established. The quantification is performed with the use of Mathworks Matlab software. For the measurements in Supplementary Fig. 5, the cell was discharged/charged at 1C rate (300 mA g^{-1}) between 0.5 and 1.4 V and the gas evolution was monitored *operando* by mass spectrometry.

DOI: 10.1038/NENERGY.2016.119

Supplementary References

(1) Chamoun, M. *et al.* Hyper-dendritic nanoporous zinc foam anodes. *NPG Asia Mater*. **7**, 178, (2015).

(4) infomine.com, Zinc Prices and Zinc Price Charts. (2016). at http://www.infomine.com/investment/metal-prices/zinc/.

(5) vanadiumcorp.com, Vanadium Electrolyte Price. (Dec 2015). at http://www.vanadiumcorp.com/tech/price.

(4) Weppner, W., Huggins, R.A. Determination of the kinetic parameters of mixed conducting electrodes and application to the system Li_3Sb. *J. Electrochem. Soc*., **124**, 1569-1578 (1977).

(5) Biesinger, M. C., Lau, L. W. M., Gersonb, A. R., Smart, R. S. C. Resolving surface chemical states in XPS analysis of first row transition metals, oxides and hydroxides: Sc, Ti, V, Cu and Zn. *Appl. Surf. Sci*. **257**, 887-898 (2010).